Inhibition of MAN2A1 enhances the immune response to anti-PD-L1 in human tumors

Sailing Shi[1*], Shengqing Gu[2*], Tong Han[1], Wubing Zhang[1,2], Lei Huang[1], Ziyi Li[1], Deng Pan[3], Jingxin Fu[1,2], Jun Ge[1], Myles Brown[4], Peng Zhang[1], Peng Jiang[5#], Kai W. Wucherpfennig[6#], Xiaole Shirley Liu[2#]

Affiliations:

1. Clinical Translational Research Center, Shanghai Pulmonary Hospital, School of Life Science and Technology, Tongji University, Shanghai, 200092, China.
2. Department of Data Sciences, Dana-Farber Cancer Institute, Harvard T.H. Chan School of Public Health, Boston, MA, 02215, USA.
3. Department of Basic Medical Sciences, Tsinghua University, Beijing, 100084, China.
4. Department of Medical Oncology, Dana-Farber Cancer Institute and Harvard Medical School, Boston, MA, 02215, USA.
5. Cancer Data Science Laboratory, National Cancer Institute, National Institutes of Health. Bethesda, MD, 20892, USA.
6. Department of Cancer Immunology and Virology, Dana-Farber Cancer Institute, Boston, MA, 02215, USA.

*These authors contributed equally to this work.

Running title: N-Glycosylation modulates tumor response to anti-PD-L1

#Corresponding Authors:
Peng Jiang (P.J.)
Mailing address: Center for Cancer Research, National Cancer Institute, Building 10, Room 6N119, Bethesda, MD, 20892
Phone number: 240-858-3799
E-mail: peng.jiang@nih.gov

Kai W. Wucherpfennig (K.W.W)
Mailing address: Dana-Farber Cancer Institute, 450 Brookline Avenue, BP332A, Boston, MA, 02215
Phone number: 617-632-3086
E-mail: kai_wucherpfennig@dfci.harvard.edu

Xiaole Shirley Liu (X.S.L.)
Mailing address: Dana-Farber Cancer Institute, 450 Brookline Avenue, BP332A, Boston, MA, 02215
Phone number: 617-632-2472
E-mail: xsliu@ds.dfci.harvard.edu

Conflict of interest.

X.S.L. is a cofounder, board and SAB member of GV20 Oncotherapy, SAB of 3DMed Care, consultant for Genentech, stock holder of BMY, TMO, WBA, ABT, ABBV, and JNJ, and

received research funding from Takeda and Sanofi.. K.W.W. is a co-founder of Immunitas, and serves on the scientific advisory board of TCR2 Therapeutics, T-Scan Therapeutics, SQZ Biotech, Nextechinvest and receives sponsored research funding from Novartis. These activities are not related to the research reported in this publication. M.B. is a consultant to and receives sponsored research support from Novartis. M.B. is a consultant to and serves on the scientific advisory boards of Kronos Bio, H3 Biomedicine, and GV20 Oncotherapy. The remaining authors declare that they have no competing interests.

Statement of Translational Relevance

Immune checkpoint blockade (ICB) has shown remarkable efficacy, but in only a minority of cancer patients, suggesting the need to develop additional treatment strategies. In this study, we integrated analyses of clinical transcription profiles of human tumors and functional CRISPR screens to discover combination therapy candidates. We identified a novel target involved in glycometabolism, MAN2A1, which suppressed the sensitivity of cancer cells to T cell-mediated killing. Pharmacological inhibition of MAN2A1 by swainsonine, an indolizidine alkaloid that can be tolerated by cancer patients, synergized with anti-PD-L1 in the treatment of melanoma and lung cancer. In light of the limited efficacy of anti-PD-L1 and failed Phase II clinical trial of swainsonine on advanced or metastatic renal cell carcinoma (RCC), our study reveals a potential therapy combining the two to overcome tumor immune evasion.

Abstract

Purpose: Immune checkpoint blockade (ICB) has shown remarkable efficacy, but in only a minority of cancer patients, suggesting the need to develop additional treatment strategies. Aberrant glycosylation in tumors, resulting from the dysregulated expression of key enzymes in glycan biosynthesis, modulates the immune response. However, the role of glycan biosynthesis enzymes in anti-tumor immunity is poorly understood. We aimed to study the immunomodulatory effects of these enzymes.

Experimental Design: We integrated transcriptional profiles of treatment-naïve human tumors and functional CRISPR screens to identify glycometabolism genes with immunomodulatory effects. We further validated our findings using in vitro co-culture and in vivo syngeneic tumor growth assays.

Results: We identified *MAN2A1*, encoding an enzyme in N-glycan maturation, as a key immunomodulatory gene. Analyses of public immune checkpoint blockade trial data also suggested a synergy between MAN2A1 inhibition and anti-PD-L1 treatment. Loss of *Man2a1* in cancer cells increased their sensitivity to T cell-mediated killing. *Man2a1* knockout enhanced response to anti-PD-L1 treatment and facilitated higher cytotoxic T cell infiltration in tumors under anti-PD-L1 treatment. Furthermore, a pharmacological inhibitor of MAN2A1, swainsonine, synergized with anti-PD-L1 in syngeneic melanoma and lung cancer models, whereas each treatment alone had little effect.

Conclusions: *Man2a1* loss renders cancer cells more susceptible to T cell-mediated killing. Swainsonine synergizes with anti-PD-L1 in suppressing tumor growth. In light of the limited efficacy of anti-PD-L1 and failed phase II clinical trial on swainsonine, our study reveals a potential therapy combining the two to overcome tumor immune evasion.

Introduction

Immune checkpoint blockade (ICB), which aims to boost the host immune system to attack cancer cells, could induce durable responses in multiple cancers (*1, 2*). However, most patients develop primary or acquired resistance to immunotherapy (*3, 4*), highlighting the importance of identifying biomarkers and regulators of tumor immune response (*5*). Genomic and transcriptomic profiling of tumors has facilitated the identification of factors that may affect tumor response to ICB treatment (*6*). Multiple factors have been reported to affect ICB response and resistance, including cytotoxic T cell infiltration (*7*), mutation load (*8-10*), antigen presentation (*11-14*), PD-L1 expression (*15, 16*), gut microbiome (*17*), interferon signaling (*14, 18, 19*), PI3K pathway (*20, 21*), and beta-catenin signaling (*22*). Elucidation of these mechanisms provides important insights into the discovery of predictive biomarkers of response (*23, 24*). However, the identification of novel therapeutic strategies that improve ICB response is still a critical challenge in this field.

Protein glycosylation is a ubiquitous post-translational modification and is essential in the development and physiology of living organisms (*25*). Glycans have been found to regulate many key biological processes, including protein folding, cellular adhesion, extracellular matrix interactions, molecular trafficking and clearance, signal transduction, and endocytosis (*25-28*). Compared to the normal tissues, tumors often show altered glycosylation patterns (*29*). Aberrant glycosylation is often observed as a driver of the malignant phenotype, directly impacting key processes in tumor progression and metastasis (*29-31*). In addition, altered glycosylation in cancer cells allows new interactions with immune cells to suppress anti-tumor immunity (*32, 33*). Immune cells can sense and respond to changes in the glycans of their microenvironment via glycan-binding proteins called lectins, which often leads to the attenuation of immune activation and the induction of inhibitory immune processes (*32*). Altogether, the abnormal glycosylation in cancer cells is associated with tumor development and progression and the ability of cancer cells to evade immune surveillance (*34, 35*).

Protein glycosylation consists of two major types, namely N-linked and O-linked (*36*). N-linked glycoproteins are frequently found on secretory and membrane-bound glycoproteins, thus are accessible for therapeutic purposes (*37, 38*). A large number of cell-surface molecules involved in the innate and adaptive immune responses are N-linked glycoproteins, such as T cell co-receptors, Toll-like receptors, cytokines, and cytokine receptors (*39*). The expression and function of these glycoproteins are dependent on normal glycosylation (*39*). Changes in their glycosylation patterns may lead to impaired protein expression and function, and significant alterations in immune pathway signaling (*33, 39*). In addition, N-glycosylation is also required for some immunosuppressive receptor-ligand engagement, such as PD-1/PD-L1, B7-1/PD-L1, and PD-1/PD-L2 (*40*). Among these, the study of the N-glycosylation of PD-L1 is the most detailed and systematic (*41*). PD-L1 is highly glycosylated in the majority of cells in which it is expressed, and N-glycosylation has been shown to stabilize PD-L1 (*42*). Thus, N-linked glycosylation is a critical regulator in the tumor microenvironment and could be manipulated to enhance anti-tumor immunity.

Despite the knowledge of the regulatory effect of glycosylation in tumor progression and the

interplay of glycosylation with the immune response, how glycosylation modulates biological processes is still an open question. Thus, the development of strategies targeting key glycan modulators to improve anti-tumor immunity remains a relatively unexploited field. Given that the dysregulated gene expression of key enzymes in the glycosylation pathway is a major contributor to alterations in glycosylation patterns (*35, 36*). Glycan biosynthesis enzymes are poised to be a major source of druggable targets that can be manipulated to enhance immune response. Since N-linked glycosylation has been reported to regulate the expression and function of many cell surface glycoproteins involved in immune responses and affect the immune receptor/ligand binding (*39, 40*), we focused on genes participating in N-glycan biosynthesis. Using a large-scale data integration approach, we evaluated the association between N-glycan biosynthesis genes and resistance to T cell cytotoxicity. This effort identified a novel N-glycan biosynthesis gene as a regulator of anti-tumor immune response, which we experimentally validated as a potential target to improve ICB response.

Materials and Methods

Cell Culture and Compounds

B16F10, A375, HEK293FT, and LLC cells were maintained in complete DMEM media (10 % fetal bovine serum, 1% L-glutamine, and 1% penicillin/streptomycin). B16F10-Cas9 cells were maintained in complete DMEM media with 2.5–5 μg/ml of blasticidin. CD8 T cells isolated from mice were cultured in complete RPMI 1640 media (10% FBS, 20 mM HEPES, 1 mM sodium pyruvate, 0.05 mM 2-mercaptoethanol, 2 mM L-glutamine and 50 U/ml streptomycin and penicillin). All cell lines are tested for mycoplasma contamination.

Generation of *Man2a1* knockout GFP+ cells

To knockout *Man2a1*, CRISPR gRNA sequences targeting *Man2a1* or non-targeting control were cloned into a PLKO3G-GFP vector and confirmed by sequencing. Knockout constructs were co-transfected with pMD2.G and psPAX2 into HEK293FT cells to generate lentivirus. Transfection was performed using X-tremeGENE™ HP DNA Transfection Reagent (Roche, #6366546001) following the manufacturer's protocol. Lentivirus was collected at 48 h and 72h. Then B16F10-Cas9 cells were infected with a lentivirus driving expression of a single gRNA for 48h to inactivate *Man2a1* genes individually. Infected cells were sorted on the basis of GFP expression by BD FACS Aria II.

Western Blotting

For western blotting, cells were lysed in RIPA buffer (50mM Tris-HCl (pH7.5), 150mM NaCl, 1% NP-40, 2mM EDTA, 0.5% Na Deoxycholate, 0.1% SDS) supplemented with protease and phosphatase inhibitor cocktail (Cell Signaling Technology, #5872s). Protein concentrations were measured with BCA Protein Assay Kit (Sangon Biotech, #C503021). For Western blotting, equal amounts of protein were heat denatured in the presence of a reducing agent and separated on 4-12% or 10% Bis-Tris SurePAGE™ gels (GeneScript, #M00652, #M00665), and transferred to PVDF membranes. Antibodies used for Western blotting were as follows: anti-mouse MAN2A1 Antibody (Santa Cruz Biotechnology, #sc-376909), anti-human MAN2A1 antibody (Santa Cruz Biotechnology, #sc-377204), pSTAT1 (Cell Signaling Technology, #9167), STAT1(Cell Signaling Technology, #9172), ERK2 (Santa Cruz,

#sc-1647), GAPDH (Sigma, #G9545), PD-L1 (E1L3N®) XP® Rabbit mAb (Cell Signaling Technology, #13684T), vinculin (Santa Cruz Biotechnology, #sc-73614), Goat anti-rabbit secondary antibody (Cell Signaling Technology, #7074s), and Goat anti-mouse secondary antibodies (Cell Signaling Technology, #7076s). The blots were imaged using CLINX imaging system according to the manufacturer's instruction.

In vitro T cell co-culture assay

Pmel-1 TCR transgenic mice were purchased from Jackson Laboratory (stock no. 005023). CD8 T cells were isolated from spleen and lymph nodes from Pmel-1 TCR transgenic mice using the EasySep mouse CD8+ T cell isolation kit (STEMCELL #19753) according to the manufacturer's protocol. Freshly isolated CD8 T cells were stimulated with anti-CD3/CD28 beads (Thermo Fisher Scientific, #11452D) at a bead to cell ratio of 1:2. On day 3, Recombinant mouse IL-2 (Biolegend, #575406) was added to the culture at 20ng/ml. The animal experiments have complied with all relevant ethical regulations. The study protocol was approved by the Institutional Care and Use Committee at Dana Farber Cancer Institute.
For optimal killing by Pmel-1 T cells, B16F10 cells were pretreated with 10ng/ml IFN- γ for 24 hours prior to co-culture to enhance MHC-I expression. In a competition assay, *Man2a1*-knockout cells or non-targeting control B16F10-Cas9 cells (GFP positive) were mixed with parental B16F10-Cas9 cells (GFP negative) at a 1:1 ratio. Mixed cells were then co-cultured with in vitro-activated Pmel-1 T cells at effector-to-target ratios of 1:0, 1:1 1:2, or 1:3. There were three cell-culture replicates for each condition. After a three-day co-culture with T cells, the percentage of GFP positive cells was determined by FACS. T cells present in these cultures were gated out on the basis of antibodies specific for CD45 (APC–Cy7) (Biolegend, #103115).

N-glycan profiling

$5*10^6$ cells were used as starting material and are lyophilized. The lyophilized proteins were digested into peptides by trypsin (Sigma-Aldrich) and then treated with PNGase F (New England Biolabs) to release N-Glycans. The released N-glycans were collected, pooled, and lyophilized. The lyophilized N-glycan samples were incubated with 1 ml of a NaOH/DMSO (Dimethyl Sulfoxide; Sigma-Aldrich)-NaOH (Sigma-Aldrich) slurry solution and 500 µl of methyl iodide (Sigma-Aldrich) for 30 min to permethylate the N-glycans. The permethylated N-glycans were then loaded into a conditioned (1 CV methanol, 1 CV MilliQ water, 1 CV acetonitrile (Sigma-Aldrich), and 1 CV Milli-Q Water) C18 50 mg Sep-Pak column. The C18 column was washed with 3 ml of 15% acetonitrile and then eluted with 3 ml of 50% acetonitrile. The eluted fraction was lyophilized and then redissolved in 15 µl of 75% methanol from which 1 µl was mixed with 1 µl DHB (2,5-dihydroxybenzoic acid (Sigma-Aldrich)) and spotted on a MALDI polished steel target plate (Bruker). MS data was acquired on a Bruker UltraFlex II MALDI-TOF Mass Spectrometer instrument. Reflective positive mode was used and data recorded between 500 m/z and 6000 m/z. MS profiles represent the aggregation of at least 20,000 laser shots. Mass peaks were annotated and assigned to N-glycans when a match was found. MS data was further analyzed and processed with mMass (Strohalm, et al. 2008).

In vivo experiments

$1x10^6$ B16F10 or LLC cells were resuspended in Hanks balanced salt solution (Gibco, #14170112) and subcutaneously injected into the right flank of 6 to 8 weeks old female C57BL/6 mice. Anti-PD-L1 (Bio X Cell, clone 10F.9G2, #BE0101, 100μg/mouse) mAbs and IgG isotype control antibodies (BioX Cell, clone LTF-2, #BE0090, 100μg/mouse) were administered on day 6, 9, 12. For the drug combination experiment, mice were treated with swainsonine (APExBIO, #B7316) by oral gavage daily in 1mg/kg/day from day 6 for 2 weeks. For CD8 depletion studies, anti-CD8 (Bio X Cell, clone YTS 169.4, #BE0117,150μg/mouse) were administered 1 day prior to treatment and then every 3 days for a total of 3 doses. Tumors were measured every 3 days beginning on day 6 after tumor challenge until the survival endpoint was reached. Measurements were assessed manually by assessing the longest dimension (length) and the longest perpendicular dimension (width). Tumor volume was calculated using the formula $1/2 \times \text{length} \times \text{width}^2$. All mouse experiments were carried out at the Shanghai Model Organisms Center. The mouse experiments were approved by the Institutional Animal Care and Use Committee of the Institute of Biochemistry and Cell Biology and performed in accordance with this committee's guidelines.

FACS analysis with tumor-infiltrating lymphocytes cells

B16F10 cells were subcutaneously injected into 6 to 8 weeks old female C57BL/6 mice. Mice were administrated with anti-PD-L1 or IgG Isotype Control starting from day 6 and then every third day. For the drug combination experiment, mice were treated with swainsonine (APExBIO, #B7316) by oral gavage daily in 1mg/kg/day from day 6. Tumors were harvested on day 15, weighed, dissected into small pieces, and incubated with 0.1% Collagenase Type I (Invitrogen, #17100-017) supplemented HBSS medium (Gibco, #2005368) for 20 min at 37 °C. After incubation, tumor cells were passed through 70-μm filters to remove the undigested tumors. Single-cell suspensions were stained with the following antibodies: BD Horizon Fixable viability stain 450 (BD Pharmingen, #562247), Ms CD45 Percy-cy5.5 30-F11 (BD Pharmingen, #550994), APC anti-mouse CD3 (Biolegend, #100236), FITC anti-mouse CD4 (Biolegend, #100405), FITC anti-mouse CD8a (Biolegend, #100705), APC anti-mouse NK1.1 (Biolegend, #108709), FITC anti-mouse F4/80 (Biolegend, #123107), Ms CD86 PE GL1 (BD Pharmingen, #561963), CD206(MMR) Monoclonal antibody (MR6F3) PE (eBioscience, #12-2061-80). BD FACSVerse was used for data acquisition, and FlowJo was used for data analysis.

Cytokine analysis from tumor lysate

Tumors were isolated from mice on day 15 after inoculation. One hundred milligrams of tissues were collected in a tube with pre-chilled 500 μl of cell lysis buffer (50mM Tris-HCl (pH 8.0), 150mM NaCl, 0.5% NP40, 10% Glycerol) supplemented with 1 mM PMSF and cOmplete Protease Inhibitor Cocktail tablets (Roche, #11836153001). Tissues were first homogenized by tissue tearor. Then ultrasonic homogenization was performed by ultrasonic homogenizer with sonication duration for 60 seconds, at an ultrasonic cycle mode of 3 seconds sonication, and 3 seconds resting time. Then the samples were centrifuged at 12,000g for 20 min at 4 °C. Protein concentration was assessed by BCA assay (Sangon Biotech, C503021). Lysates were then probed for IFN-γ (ExCell Bio, #EM007-96, sensitivity:

4pg/mL) and TNF-α (ExCell Bio, #EM008-96, sensitivity: 7pg/mL) protein levels by ELISA.

RNA-Seq data analysis

RNA was extracted using TRIzol reagent (Invitrogen Life Technologies, Gaithersburg, MD, USA) according to the manufacturer's instructions. Quality and quantity of RNA were analyzed using NanoDrop, agarose gel electrophoresis, and Agilent 2100 (Thermo Fisher Scientific, MA, USA). Oligo(dT)-attached magnetic beads were used to purify mRNA. Purified mRNA was fragmented into short fragments with fragment buffer, and cDNAs were synthesized using the RNA fragments as templates for random primer, followed by end reparation and ligation to adapters. The cDNA libraries for B16F10 cancer cell line were sequenced using Illumina Nova 6000 by Berry Genomics Co. Ltd. For B16F10 tumors, the libraries were sequenced on BGIseq500 platform (BGI-Shenzhen, China). Data were aligned to mouse reference genome mm10 using STAR. RSEM was used to map aligned reads and to generate a gene count matrix. Differential expression was performed using Deseq2. We performed gene set enrichment analysis using "MAGeCKFlute" R package (*43*) and GSEA pre-ranked mode (*44*).

Histopathology analysis of internal organs

Mouse tissues were perfusion fixed in 4% paraformaldehyde solution overnight, and then embedded in paraffin. Four-micrometer thick sections were cut and stained with hematoxylin and eosin (H&E). H&E-stained tissue sections were imaged using NIKON ECLIPSE CI. The pathology of mouse colon and liver sections were scored by referring to McGuckin's (*45*) and Ishak's (*46*) standards respectively, and were scored double-blind. The toxicity score for each organ is the sum of individual scores.

Data processing for publicly available datasets

The method to calculate the T cell dysfunction score was described in the TIDE algorithm, which we published before (*47*). Briefly, the interaction test in multivariate Cox-PH regression was applied to identify gene association with the T cell dysfunction phenotype. The T cell dysfunction score for each gene is defined as the Wald test z score. For visualization purposes, samples were split to optimize the expression coefficients of interested genes in the Cox-PH regression model. However, the p-value significance computation was continuous without any cutoffs. The CTL level was estimated through bulk-tumor expression average of CD8A, CD8B, GZMA, GZMB, and PRF1. For public T cell co-culture screen analysis, the raw count was downloaded, and MAGeCK (*48*) was used to compute the log2 fold change for all gRNAs by comparing the experimental and control conditions.

Statistics.

Statistical tests employed with the number of replicates and independent experiments are listed in the text and figure legends. Statistical analyses were performed either with the R software (http://www.R-project.org/) or Prism 6 (GraphPad, San Diego, CA, USA). Statistical analyses gathering more than two groups were performed using ANOVA. Otherwise, for two groups, statistical analyses were performed using the unpaired t-test. Log-rank test was applied when assessing the impact of the treatment on mice survival. Multiple hypothesis

testing corrections were applied where multiple hypotheses were tested and were indicated by the use of FDR.

Result

MAN2A1 is associated with T cell dysfunction

Previously our group developed a computational model TIDE (Tumor Immune Dysfunction and Exclusion) (*47*), which integrated the expression signatures of T cell dysfunction and T cell exclusion to evaluate tumor immune evasion and predict response to ICB. TIDE examined 188 clinical study cohorts with expression profiles and clinical outcome information of over 33K cancer samples from the TCGA (*49*), PRECOG (*50*), and METABRIC (*51*) databases. To model T cell dysfunction, TIDE applied a Cox-PH regression to compute how the expression of each gene interacts with cytotoxic T lymphocyte infiltration to influence patient survival. To model T cell exclusion, TIDE calculated the gene expression correlation with that of three immunosuppressive cell types reported to restrict T cell infiltration into tumors. Recently, we significantly expanded the scope of TIDE by incorporating many new datasets and functional modules (*52*). We integrated nearly 1,000 omics data from 12 published ICB clinical studies and 8 published CRISPR screens that identified genes that regulate lymphocyte-driven cancer killing and/or immunotherapy response. These efforts in the reuse of public data significantly improved the power of TIDE in hypothesis generation and enabled us to identify novel genes with immunomodulatory effects.

Because N-linked glycoproteins are essential to the antigen presentation and subsequent triggering of T cell-mediated immune responses (*53*), we evaluated all the N-glycan biosynthesis genes through TIDE to identify their association with T cell dysfunction. Several genes in this pathway **(Supplementary Table. S1)**, such as *MGAT5*, *MAN1C1*, and *MAN2A1*, showed high T cell dysfunction scores across multiple cohorts **(Fig. 1A)**. High expression of these genes is negatively associated with cytotoxic T cell-mediated survival benefit **(Fig. 1B; Supplementary Fig. S1)**, suggesting that T cells might be dysfunctional when these genes are highly expressed in the tumor microenvironment. To distinguish whether these genes are regulators or merely markers of T cell dysfunction, we examined public CRISPR screens in mouse cancer cells co-cultured with mouse primary T cells that specifically target the cancer cell antigen. Based on five such screens from two independent studies (*54, 55*), we found that gRNAs targeting *Man2a1* were consistently negatively selected **(Fig. 1C)**. These results implicated *MAN2A1* as a regulator of T cell dysfunction, whose inactivation may sensitize cancer cells to T cell-mediated lysis.

MAN2A1 encodes a glycosyl hydrolases that is normally expressed in Golgi and catalyzes the final step in the N-linked glycan maturation pathway (*56*). To evaluate in which cancer type(s) MAN2A1 regulates the response to T cell-driven cytotoxicity, we examined the expression of MAN2A1 in patient samples using publicly available databases, such as TCGA and NCBI GEO. We found *MAN2A1* is expressed at a higher level in tumor tissues of melanoma and lung cancer as compared to their adjacent normal tissues **(Supplementary Fig.S2A-S2D)**. In addition, *MAN2A1* showed high T cell dysfunction scores in most of the

melanoma and lung cancer cohorts **(Supplementary Fig.S2E and S2F)**. These data suggest that MAN2A1 may promote the resistance to T cell-mediated killing in melanoma and lung cancer.

***Man2a1*-null cancer cells are more sensitive to T cell-mediated killing**

To validate the function of *Man2a1* in T cell-mediated tumor killing, we transduced B16F10-Cas9 cells with lentivirus co-expressing GFP and CRISPR guide RNAs (gRNA) targeting *Man2a1*. Western blot experiment confirmed the diminished level of MAN2A1 in the knockout cell line **(Fig. 2A)**. Next, *Man2a1*-null or control sgRosa26 B16F10 cells (GFP-positive) were mixed with equal number of parental B16F10 cells (GFP-negative), and co-cultured with in vitro-activated Pmel-1 T cells at different ratios. After three days of co-culture, the percentage of *Man2a1*-null B16F10 cells in the presence or absence of T cells was determined by FACS (**Fig. 2B; Supplementary Fig. S3**). Consistent with the public co-culture CRISPR screen result, *Man2a1*-null B16F10 cells were significantly more sensitive to T cell-mediated cytotoxicity compared with sgRosa26 control cells **(Fig. 2C)**.

$CD8^+$ T cell-mediated tumor attack involves the secretion of key cytokines, such as IFN-γ and TNF-α, to induce proliferative arrest or apoptosis signaling (*57*). Suppression of cytokine signaling is one of the key mechanisms by which tumors evade attack by cytotoxic T cells (*55, 58*). To investigate whether *Man2a1* depletion sensitized B16F10 cells to T cell-mediated killing via the IFN-γ signaling, we examined the responsiveness of cancer cells to IFN-γ treatment. The biological effects of IFN-γ are elicited mainly through the activation of the JAK / STAT pathway (*59*). *Man2a1*-knockout cells exhibited no significant difference from the control cells in the induction of STAT1 signaling upon IFN-γ treatment, as measured by the phosphorylation status of STAT1 **(Supplementary Fig. S4A)**. In addition, mouse *Man2a1*-null B16F10 cells and human *MAN2A*1-null A375 cells showed no significant proliferative difference compared to their respective control cells in response to IFN-γ **(Supplementary Fig. S4B and S4C)**. Similarly, loss of MAN2A1 in these cells had no significant impact on the growth inhibition by either TNF-α alone or combined treatment of IFN-γ and TNF-α **(Supplementary Fig. S4D and S4E)**. Collectively, these data suggest that the enhanced sensitivity to T cell-mediated killing through *Man2a1* knockout is not mediated by enhanced sensitivity to IFN-γ or TNF-α by cytokine-intrinsic mechanisms, implying instead potentially novel mechanisms of this phenomenon.

***Man2a1* knockout changes glycometabolism**

To investigate how *Man2a1* knockout regulates cancer cell sensitivity to T cell-driven cytotoxicity, we examined the transcriptome of *Man2a1*-null B16F10 cells by RNA-seq. *Man2a1* knockout in B16F10 cells did not induce any marked gene expression change in the immune-related pathways **(Supplementary Table. S2)**. Interestingly, genes involved in the glyco-metabolic pathways, such as glycolysis, starch and sucrose metabolism, and galactose metabolism, were concordantly downregulated in *Man2a1*-knockout cells **(Fig. 3A and B)**, indicating that *Man2a1* loss may impact cancer cell glycometabolism. *MAN2A1* encodes α-mannosidase II, a key enzyme in the N-glycan biosynthesis that converts precursor high mannose type N-glycans to matured complex-type structures (*60*). Glucose is necessary for

glycosylation through its utilization in the hexosamine biosynthetic pathway, which produces UDP-N-acetylglucosamine (UDP-GlcNAc), the substrate for glycosylation (*61*). Thus, *Man2a1* knockout might change glucose metabolism through the utilization of glucose in the N-glycan biosynthesis process.

Of note, we did not observe significant expression changes in the N-glycan biosynthesis pathway or protein N-glycosylation pathway upon *Man2a1*-knockout **(Supplementary Table. S2)**, which is expected because N-glycosylation is a post-translational modification. To examine the effect of *Man2a1*-knockout on N-glycan changes, we used mass spectrometry to evaluate the relative abundance of N-glycan component in the B16F10 cells. Consistent with MAN2A1's known function, upon *Man2a1*-knockout, simple/precursor type **(Supplementary Fig. S5A)** and hybrid type **(Fig. 3C)** N-glycans increased, while complex type N-glycans decreased **(Fig. 3D)**. In contrast, bisected **(Supplementary Fig. S5B)** and high mannose type **(Supplementary Fig. S5C)** N-glycans showed no significant change. Given that *MAN2A1* knockout changes the N-glycan composition, we hypothesized that loss of *MAN2A1* might alter the glycosylation pattern of some cell surface glycoproteins, thus affecting the interaction with T cells. Li *et al.* reported that inhibitors blocking N-linked glycosylation, such as swainsonine, altered the glycosylation of PD-L1 and reduce the PD-1/PD-L1 interaction(*40*). Glycosylation of PD-L1 is essential to the immune inhibitory effect of PD-L1, and non-glycosylated PD-L1 is unable to bind to PD-1 (*40*). Cells expressing non-glycosylated PD-L1 are more sensitive to T cell-mediated killing (*40*). Indeed, we found that the molecular weight of PD-L1 in *MAN2A1*-knockout or swainsonine-treated cells was lower than in control cells, while expression remained similar **(Fig. 3E and F; Supplementary Fig. S6)**, consistent with its altered glycosylation. These data demonstrate that the immunomodulatory effect of MAN2A1 is associated with global glycosylation changes, consistent with reported effects of altered PD-L1 glycosylation.

***Man2a1* loss in cancer cells enhances anti-PD-L1 response**

Lee and colleagues have demonstrated that N-linked glycosylation of PD-L1 hinders its binding with PD-L1 antibodies, and the removal of N-linked glycosylation enhances its predictive value for anti-PD1/PD-L1 efficacy (*62*). We therefore asked whether *MAN2A1* knockout would influence the efficacy of ICB treatment. To study the association between *MAN2A1* and tumor ICB response, we used the down regulated genes in *Man2a1*-knockout cells to generate a signature. Then we used this signature as a proxy for *MAN2A1* activity to test its association with response to ICB. Out of the five clinical cohorts we collected, we found lower MAN2A1 activity to be associated with better response and better overall survival in a large anti-PD-L1 trial (*63*) **(Fig. 4A and B)**, but not consistently in the anti-PD-1 (*64-66*) or anti-CTLA-4 trials (*7*) **(Supplementary Fig. S7).** These data suggest that inhibition of *MAN2A1* might improve tumor response to anti-PD-L1.

To test whether *Man2a1* knockout synergizes with anti-PD-L1 treatment *in vivo*, we used the B16F10 syngeneic tumor model that is resistant to current ICB (*66-68*). *Man2a1*-null B16F10 tumors showed similar growth with non-targeting control B16F10 tumors when treated with IgG isotype control antibody **(Fig. 4C)**. However, PD-L1 blocking antibody conferred

therapeutic benefit in mice bearing *Man2a1*-null B16F10 tumors but this treatment was ineffective against control B16F10 tumors **(Fig. 4C and D)**. Altogether, these data indicate that inactivation of *Man2a1* in cancer cells could sensitize tumors to anti-PD-L1 immunotherapy.

Man2a1 knockout increases the cytotoxic immune cell infiltration and activities

To better understand the effect of *Man2a1* depletion on the tumor microenvironment, we performed RNA-seq and flow cytometry on the syngeneic tumors in each of the above four conditions. RNA-seq analysis found immune-related pathways, such as lymphocyte migration and activation, adaptive immune response, cytokine and chemokine signaling, and IFN-γ production, to be significantly enriched in the *Man2a1*-null tumors treated with anti-PD-L1 **(Fig. 5A; Supplementary Table. S3)**. In addition, up-regulation of genes involved in antigen presentation, inflammatory response, and T cell activation were consistently observed in *Man2a1*-null tumors with anti-PD-L1 treatment **(Fig. 5B)**. The immune-stimulatory phenomena were not observed in other conditions (**Supplementary Table. S4 and Supplementary Table. S5**), except that anti-PD-L1 treatment of the control tumors increased CD45+ lymphocytes infiltration **(Fig. 5C)**. Furthermore, *Man2a1*-null tumors had significantly increased proportions of CD3+ T cells, CD8+ T cells in response to anti-PD-L1 **(Fig. 5D and E)**, whereas CD4+ T cells, NK cells, M1 or M2 macrophages had no significant change **(Supplementary Fig. S8)**. Finally, a significant increase of IFN-γ and TNF-α protein secretion was observed **(Fig. 5F and G)**, indicating the activation of cytotoxic lymphocytes and effective tumor killing. Taken together, our data suggest that inactivation of *Man2a1* in tumors treated with anti-PD-L1 results in not only increased immune cell infiltration but also enhanced cytotoxic tumor killing.

Pharmacological inhibition of *Man2a1* sensitizes tumors to anti-PD-L1

To further evaluate the efficacy of targeting *MAN2A1*, we tested the *in vivo* effect of combined treatment of a MAN2A1 inhibitor swainsonine and anti-PD-L1 antibody. Swainsonine is a pharmacological inhibitor of α-mannosidase, and it inhibits both Golgi alpha-mannosidase and lysosomal alpha mannosidase (*69*). It has been shown to stimulate lymphocyte proliferation, enhance T cell stimulation by antigen, and activate natural antitumor immunity (*70, 71*). Furthermore, it has been shown to inhibit tumor growth and metastasis in hepatocellular carcinoma (*72*), melanoma (*73, 74*), and lymphoma (*75*) mouse models. Although swainsonine had promising results in initial clinical settings (*76, 77*), it failed a phase II clinical trial on advanced or metastatic renal cell carcinoma (RCC) due to limited efficacy (*78*). In B16F10 tumors, co-administration of swainsonine and anti-PD-L1 significantly enhanced the anti-tumor effects and survival benefits, whereas anti-PD-L1 or swainsonine treatment alone had little impact on tumor growth or mouse survival **(Fig. 6A and B)**. We also tested this synergistic effect in the LLC lung cancer model and observed similar effects **(Fig. 6C and D)**. Notably, depletion of CD8+ T cells by anti-CD8 treatment significantly abrogated the anti-tumor effects of anti-PD-L1 and swainsonine combination therapy **(Fig. 6C and D),** suggesting that CD8+ T cells play important roles in the tumor rejection effect of the combination therapy.

To further characterize the enhanced immune response to combination therapy, we performed flow cytometry and RNA-seq of B16F10 tumors treated with either monotherapy or combination therapy. Flow cytometry analysis showed a significant increase of tumor-infiltrating CD3+ and CD8+ T cells in tumors receiving anti-PD-L1 plus swainsonine **(Fig. 6E and F)**, whereas CD4+ T cells, NK cells, M1 or M2 macrophages had no significant change **(Supplementary Fig. S9)**. RNA-seq analysis revealed up-regulation of immune-related pathways, such as adaptive immune response, IFN-γ production, T cell activation, and cytokine secretion, in tumors treated with combined anti-PD-L1 and swainsonine relative to tumors treated with either monotherapy or control antibody **(Fig. 6G, Supplementary Table. S6 and Supplementary Table. S7)**. Up-regulation of gene signatures associated with T cell activation and leukocyte mediated cytolysis was also observed in tumors treated with the combination therapy **(Fig. 6H)**. In addition, both IFN-γ and TNF-α protein levels were significantly higher in tumors treated with the combination therapy, consistent with enhanced T cell function **(Fig. 6I and J)**. Altogether, our findings suggest that swainsonine may be combined with anti-PD-L1 immunotherapy to enhance anti-tumor immunity.

Patients receiving combination immunotherapy are at an increased risk of immune-related adverse events (irAEs) (*79*). Although fatal high-grade irAEs are rare, adverse events remain a major limitation of checkpoint blockade and frequently result in treatment termination. To evaluate whether the combination of anti-PD-L1 and swainsonine would aggravate irAEs, we harvested organs from B16F10 tumor-bearing mice that had received either monotherapy or combination therapy. Examination of tissue sections revealed a pathology of low/moderate portal and lobular inflammation in the liver as well as moderate colon inflammation with anti-PD-L1 monotherapy **(Supplementary Fig. S10)**. Colon and liver inflammation was not worsened by combination therapy with anti-PD-L1 and swainsonine compared to anti-PD-L1 monotherapy **(Supplementary Fig. S10)**. No significant histological changes were observed in the spleen in any of the treatment groups **(Supplementary Fig. S10)**. These preclinical safety data demonstrate that the addition of swainsonine did not increase inflammatory lesions associated with anti-PD-L1 therapy.

Discussion

Cancer treatment by immune checkpoint blockade (ICB) achieved striking successes in the last decade, but the majority of patients do not respond (*80*). Although N-glycosylation has been known to be important for cancer immunology, previous studies haven't identified the key regulators that can be targeted to improve immunotherapy efficacy. In this study, we used a comprehensive data integration approach to identify and *in vitro* experiments to characterize *MAN2A1*, encoding an enzyme involved in N-glycan maturation, as a novel target to sensitize tumors to T cell-mediated cytotoxicity. *Man2a1* loss changed the overall glycosylation pattern in cancer cells, and *Man2a1* knockout in cancer cells rendered B16F10 tumors sensitive to PD-L1 blockade therapy and activated the tumor immune microenvironment. We also identified that swainsonine, an inhibitor of alpha-mannosidase II, might be an ideal drug that can be combined with anti-PD-L1 immunotherapy to enhance immune response. The synergy we observed between anti-PD-L1 and swainsonine in vivo, whereas each treatment alone had little effect, is an important finding. This is especially of

potential clinical significance, in light of the limited efficacy of anti-PD-L1 and failed clinical trial on swainsonine, and underlies the importance of data integration on cancer immunology studies.

Previous studies reported that *Man2a1*-null mice exhibited a three-fold increase in the abundance of hybrid type N-glycans and approximately half the level of complex type N-glycans (*60*). Aged mice with constitutive *Man2a1* deficiency show systemic autoimmune disease similar to human systemic lupus erythematosus (*81*), although lymphoid lineage development and activation responses were unaffected (*82*). The autoimmune syndrome of *Man2a1*-deficient mice can be explained by a pathogenic pro-inflammatory condition in the absence of infection due to the aberrant synthesis of endogenous glycans (*37, 82*). These symptoms indicated a prominent role of endogenous α-mannosidase II in the regulation of inflammatory immune responses. We also observed the immune stimulatory signaling in mice injected with *Man2a1*-null B16F10 tumors treated with anti-PD-L1 but not in those treated with IgG isotype control antibody. The lack of immune stimulation with *Man2a1* inhibition alone in the B16F10 model and maybe other tumors might explain the reason why swainsonine failed the previous clinical trial. Our data suggests that anti-PD-L1 treatment might enhance the pro-inflammatory benefit of *MAN2A1* inhibition.

There are several limitations of our study. First, in the B16F10 and LLC model we tested, *Man2a1* inhibition alone does not affect tumor growth and tumor microenvironment. However, other studies reported tumor growth rejection and immune stimulation with swainsonine treatment alone (*83*), suggesting that *Man2a1* may have strong effect in other tumor models. Second, we observed reduced molecular weight of PD-L1 in *MAN2A1*-knockout and swainsonine treated cells, suggesting the impaired glycosylation of PD-L1. Previous studies demonstrated that glycosylation of PD-L1 is necessary for PD-1/PD-L1 interaction (*40*), and impedes the binding with anti-PD-L1 antibodies (*62*). Thus, we hypothesized that PD-L1 expressed in *MAN2A1*-null cells might have lower binding affinity with PD-1, thus reducing the suppression of T cell activity by PD-1/PD-L1 interaction and enhancing the sensitivity to T cell killing. Moreover, MAN2A1 knockout may also affect the glycosylation of other immuno-regulatory proteins and influence the function of these glycoproteins and also the interaction of important immune receptor/ligand. Changes of the glycosylation pattern of immuno-modulatory glycoproteins might impact the activity of multiple immune cells and immune responses, such as antigen presentation and T cell priming (*32*). However, additional detailed experiments are needed to fully elucidate the full mechanism. Third, single cell RNA-Seq (scRNA-seq) provides an unbiased profiling of immune cells and enables us to study the clonal expansion, migration, and functional state transition of T cells or other immune cells in the tumor microenvironment (*84, 85*). Although tumor bulk RNA-seq revealed the up-regulation of pro-inflammatory pathways in *Man2a1*-null tumors in response to anti-PD-L1 and B16F10 tumors treated with the combined anti-PD-L1 and swainsonine, scRNA-seq will allow us to systematically study the tumor microenvironment and gene expression changes induced by *Man2a1* knockout at finer resolution. While there have been numerous scRNA-seq studies published on tumors, some treated with ICB, none were on tumors treated with anti-PD-L1. Finally, swainsonine treatment could sensitize tumors to

anti-PD-L1 treatment. However, swainsonine might affect the glycosylation pattern of other cells in the tumor microenvironment or in normal tissues besides cancer cells, and these effects deserve more detailed characterization.

Despite these limitations, our discovery that inhibition of *MAN2A1* sensitizes tumors to PD-L1 blockade therapy represents the first work identifying a regulator in the N-glycan biosynthesis pathway that can be targeted to improve ICB response. Our work not only lays the foundation for the combination of *MAN2A1* inhibitor and anti-PD-L1 antibody to improve response in future cancer therapeutics, but also sets the bridge for immunology and glycobiology. Manipulation of glycosylation might be an effective strategy to improve ICB response and overcome current limitations in the treatment of cancer.

Data availability

All data presented in this manuscript are available from the corresponding author upon reasonable request. RNA sequencing data has been deposited at the Gene Expression Omnibus (GEO) under accession number GSE152925.

Acknowledgments

This work was partially supported by NIH R01CA234018 and the National Natural Science Foundation of China (81872290).

Author Contributions

S.S., S.G., P.J., and X.S.L. designed the study. S.S., S.G., T.H., and L.H. performed all the experiments. S.S., W.Z., and J.G. analyzed the RNA-Seq and T cell co-culture CRISPR screen data. J.F. collected and analyzed the clinical data. X.S.L., K.W.W., P.J., M.B., T.X., Z.L., and D.P. helped with technical clarifications and result interpretations. S.S., S.G., and X.S.L. wrote the manuscript. All authors contributed to the discussion and revision of the manuscript.

References

1. L. Chen, X. Han, Anti-PD-1/PD-L1 therapy of human cancer: past, present, and future. *J Clin Invest* **125**, 3384-3391 (2015).
2. S. H. Baumeister, G. J. Freeman, G. Dranoff, A. H. Sharpe, Coinhibitory Pathways in Immunotherapy for Cancer. *Annu Rev Immunol* **34**, 539-573 (2016).
3. A. Kalbasi, A. Ribas, Tumour-intrinsic resistance to immune checkpoint blockade. *Nat Rev Immunol*, (2019).
4. P. Sharma, S. Hu-Lieskovan, J. A. Wargo, A. Ribas, Primary, Adaptive, and Acquired Resistance to Cancer Immunotherapy. *Cell* **168**, 707-723 (2017).
5. D. S. Chen, I. Mellman, Elements of cancer immunity and the cancer-immune set point. *Nature* **541**, 321-330 (2017).
6. L. J. van 't Veer *et al.*, Gene expression profiling predicts clinical outcome of breast cancer. *Nature* **415**, 530-536 (2002).
7. E. M. Van Allen *et al.*, Genomic correlates of response to CTLA-4 blockade in metastatic melanoma. *Science* **350**, 207-211 (2015).
8. A. Snyder *et al.*, Genetic basis for clinical response to CTLA-4 blockade in melanoma.

N Engl J Med **371**, 2189-2199 (2014).
9. R. M. Samstein *et al.*, Tumor mutational load predicts survival after immunotherapy across multiple cancer types. *Nat Genet* **51**, 202-206 (2019).
10. N. A. Rizvi *et al.*, Cancer immunology. Mutational landscape determines sensitivity to PD-1 blockade in non-small cell lung cancer. *Science* **348**, 124-128 (2015).
11. M. Sade-Feldman *et al.*, Resistance to checkpoint blockade therapy through inactivation of antigen presentation. *Nat Commun* **8**, 1136 (2017).
12. F. M. Marincola, E. M. Jaffee, D. J. Hicklin, S. Ferrone, Escape of human solid tumors from T-cell recognition: molecular mechanisms and functional significance. *Adv Immunol* **74**, 181-273 (2000).
13. A. Sucker *et al.*, Genetic evolution of T-cell resistance in the course of melanoma progression. *Clin Cancer Res* **20**, 6593-6604 (2014).
14. J. M. Zaretsky *et al.*, Mutations Associated with Acquired Resistance to PD-1 Blockade in Melanoma. *N Engl J Med* **375**, 819-829 (2016).
15. M. Nishino, N. H. Ramaiya, H. Hatabu, F. S. Hodi, Monitoring immune-checkpoint blockade: response evaluation and biomarker development. *Nat Rev Clin Oncol* **14**, 655-668 (2017).
16. K. Shien, V. A. Papadimitrakopoulou, Wistuba, II, Predictive biomarkers of response to PD-1/PD-L1 immune checkpoint inhibitors in non-small cell lung cancer. *Lung Cancer* **99**, 79-87 (2016).
17. B. Routy *et al.*, Gut microbiome influences efficacy of PD-1-based immunotherapy against epithelial tumors. *Science* **359**, 91-97 (2018).
18. J. Gao *et al.*, Loss of IFN-gamma Pathway Genes in Tumor Cells as a Mechanism of Resistance to Anti-CTLA-4 Therapy. *Cell* **167**, 397-404 e399 (2016).
19. N. Jacquelot *et al.*, Sustained Type I interferon signaling as a mechanism of resistance to PD-1 blockade. *Cell Res* **29**, 846-861 (2019).
20. W. Zheng, J. W. Pollard, Inhibiting macrophage PI3Kgamma to enhance immunotherapy. *Cell Res* **26**, 1267-1268 (2016).
21. O. De Henau *et al.*, Overcoming resistance to checkpoint blockade therapy by targeting PI3Kgamma in myeloid cells. *Nature* **539**, 443-447 (2016).
22. S. Spranger, R. Bao, T. F. Gajewski, Melanoma-intrinsic beta-catenin signalling prevents anti-tumour immunity. *Nature* **523**, 231-235 (2015).
23. J. J. Havel, D. Chowell, T. A. Chan, The evolving landscape of biomarkers for checkpoint inhibitor immunotherapy. *Nat Rev Cancer* **19**, 133-150 (2019).
24. M. Luksza *et al.*, A neoantigen fitness model predicts tumour response to checkpoint blockade immunotherapy. *Nature* **551**, 517-520 (2017).
25. K. Ohtsubo, J. D. Marth, Glycosylation in cellular mechanisms of health and disease. *Cell* **126**, 855-867 (2006).
26. K. S. Lau *et al.*, Complex N-glycan number and degree of branching cooperate to regulate cell proliferation and differentiation. *Cell* **129**, 123-134 (2007).
27. S. S. Pinho, C. A. Reis, Glycosylation in cancer: mechanisms and clinical implications. *Nat Rev Cancer* **15**, 540-555 (2015).
28. S. Mereiter, M. Balmana, D. Campos, J. Gomes, C. A. Reis, Glycosylation in the Era of Cancer-Targeted Therapy: Where Are We Heading? *Cancer Cell* **36**, 6-16 (2019).

29. W. K. Cheng, C. E. Oon, How glycosylation aids tumor angiogenesis: An updated review. *Biomed Pharmacother* **103**, 1246-1252 (2018).
30. M. N. Christiansen *et al.*, Cell surface protein glycosylation in cancer. *Proteomics* **14**, 525-546 (2014).
31. M. M. Fuster, J. D. Esko, The sweet and sour of cancer: glycans as novel therapeutic targets. *Nat Rev Cancer* **5**, 526-542 (2005).
32. E. RodrIguez, S. T. T. Schetters, Y. van Kooyk, The tumour glyco-code as a novel immune checkpoint for immunotherapy. *Nat Rev Immunol* **18**, 204-211 (2018).
33. Y. van Kooyk, G. A. Rabinovich, Protein-glycan interactions in the control of innate and adaptive immune responses. *Nat Immunol* **9**, 593-601 (2008).
34. B. N. Vajaria, P. S. Patel, Glycosylation: a hallmark of cancer? *Glycoconj J* **34**, 147-156 (2017).
35. J. M. van den Elsen, D. A. Kuntz, D. R. Rose, Structure of Golgi alpha-mannosidase II: a target for inhibition of growth and metastasis of cancer cells. *EMBO J* **20**, 3008-3017 (2001).
36. A. Silsirivanit, Glycosylation markers in cancer. *Adv Clin Chem* **89**, 189-213 (2019).
37. J. D. Marth, P. K. Grewal, Mammalian glycosylation in immunity. *Nat Rev Immunol* **8**, 874-887 (2008).
38. Y. Tian, H. Zhang, Characterization of disease-associated N-linked glycoproteins. *Proteomics* **13**, 504-511 (2013).
39. J. J. Lyons, J. D. Milner, S. D. Rosenzweig, Glycans Instructing Immunity: The Emerging Role of Altered Glycosylation in Clinical Immunology. *Front Pediatr* **3**, 54 (2015).
40. C. W. Li *et al.*, Eradication of Triple-Negative Breast Cancer Cells by Targeting Glycosylated PD-L1. *Cancer Cell* **33**, 187-201 e110 (2018).
41. J. M. Hsu, C. W. Li, Y. J. Lai, M. C. Hung, Posttranslational Modifications of PD-L1 and Their Applications in Cancer Therapy. *Cancer Res* **78**, 6349-6353 (2018).
42. C. W. Li *et al.*, Glycosylation and stabilization of programmed death ligand-1 suppresses T-cell activity. *Nat Commun* **7**, 12632 (2016).
43. B. Wang *et al.*, Integrative analysis of pooled CRISPR genetic screens using MAGeCKFlute. *Nat Protoc* **14**, 756-780 (2019).
44. A. Subramanian *et al.*, Gene set enrichment analysis: a knowledge-based approach for interpreting genome-wide expression profiles. *Proc Natl Acad Sci U S A* **102**, 15545-15550 (2005).
45. C. K. Heazlewood *et al.*, Aberrant mucin assembly in mice causes endoplasmic reticulum stress and spontaneous inflammation resembling ulcerative colitis. *PLoS Med* **5**, e54 (2008).
46. K. Ishak *et al.*, Histological grading and staging of chronic hepatitis. *J Hepatol* **22**, 696-699 (1995).
47. P. Jiang *et al.*, Signatures of T cell dysfunction and exclusion predict cancer immunotherapy response. *Nat Med* **24**, 1550-1558 (2018).
48. W. Li *et al.*, MAGeCK enables robust identification of essential genes from genome-scale CRISPR/Cas9 knockout screens. *Genome Biol* **15**, 554 (2014).
49. N. Cancer Genome Atlas Research *et al.*, The Cancer Genome Atlas Pan-Cancer

analysis project. *Nat Genet* **45**, 1113-1120 (2013).
50. A. J. Gentles *et al.*, The prognostic landscape of genes and infiltrating immune cells across human cancers. *Nat Med* **21**, 938-945 (2015).
51. C. Curtis *et al.*, The genomic and transcriptomic architecture of 2,000 breast tumours reveals novel subgroups. *Nature* **486**, 346-352 (2012).
52. J. Fu *et al.*, Large-scale public data reuse to model immunotherapy response and resistance. *Genome Med* **12**, 21 (2020).
53. K. A. Wall, J. D. Pierce, A. D. Elbein, Inhibitors of glycoprotein processing alter T-cell proliferative responses to antigen and to interleukin 2. *Proc Natl Acad Sci U S A* **85**, 5644-5648 (1988).
54. D. Pan *et al.*, A major chromatin regulator determines resistance of tumor cells to T cell-mediated killing. *Science* **359**, 770-775 (2018).
55. C. J. Kearney *et al.*, Tumor immune evasion arises through loss of TNF sensitivity. *Sci Immunol* **3**, (2018).
56. K. W. Moremen, P. W. Robbins, Isolation, characterization, and expression of cDNAs encoding murine alpha-mannosidase II, a Golgi enzyme that controls conversion of high mannose to complex N-glycans. *J Cell Biol* **115**, 1521-1534 (1991).
57. M. D. Turner, B. Nedjai, T. Hurst, D. J. Pennington, Cytokines and chemokines: At the crossroads of cell signalling and inflammatory disease. *Biochim Biophys Acta* **1843**, 2563-2582 (2014).
58. D. W. Vredevoogd *et al.*, Augmenting Immunotherapy Impact by Lowering Tumor TNF Cytotoxicity Threshold. *Cell* **178**, 585-599 e515 (2019).
59. F. Castro, A. P. Cardoso, R. M. Goncalves, K. Serre, M. J. Oliveira, Interferon-Gamma at the Crossroads of Tumor Immune Surveillance or Evasion. *Front Immunol* **9**, 847 (2018).
60. D. Chui *et al.*, Alpha-mannosidase-II deficiency results in dyserythropoiesis and unveils an alternate pathway in oligosaccharide biosynthesis. *Cell* **90**, 157-167 (1997).
61. K. E. Wellen, C. B. Thompson, A two-way street: reciprocal regulation of metabolism and signalling. *Nat Rev Mol Cell Biol* **13**, 270-276 (2012).
62. H. H. Lee *et al.*, Removal of N-Linked Glycosylation Enhances PD-L1 Detection and Predicts Anti-PD-1/PD-L1 Therapeutic Efficacy. *Cancer Cell* **36**, 168-178 e164 (2019).
63. S. Mariathasan *et al.*, TGFbeta attenuates tumour response to PD-L1 blockade by contributing to exclusion of T cells. *Nature* **554**, 544-548 (2018).
64. N. Riaz *et al.*, Tumor and Microenvironment Evolution during Immunotherapy with Nivolumab. *Cell* **171**, 934-949 e916 (2017).
65. T. N. Gide *et al.*, Distinct Immune Cell Populations Define Response to Anti-PD-1 Monotherapy and Anti-PD-1/Anti-CTLA-4 Combined Therapy. *Cancer Cell* **35**, 238-255 e236 (2019).
66. W. Hugo *et al.*, Genomic and Transcriptomic Features of Response to Anti-PD-1 Therapy in Metastatic Melanoma. *Cell* **165**, 35-44 (2016).
67. S. Chen *et al.*, Combination of 4-1BB agonist and PD-1 antagonist promotes antitumor effector/memory CD8 T cells in a poorly immunogenic tumor model. *Cancer Immunol Res* **3**, 149-160 (2015).

68. A. van Elsas, A. A. Hurwitz, J. P. Allison, Combination immunotherapy of B16 melanoma using anti-cytotoxic T lymphocyte-associated antigen 4 (CTLA-4) and granulocyte/macrophage colony-stimulating factor (GM-CSF)-producing vaccines induces rejection of subcutaneous and metastatic tumors accompanied by autoimmune depigmentation. *J Exp Med* **190**, 355-366 (1999).
69. D. R. Rose, Structure, mechanism and inhibition of Golgi alpha-mannosidase II. *Curr Opin Struct Biol* **22**, 558-562 (2012).
70. S. L. White, K. Schweitzer, M. J. Humphries, K. Olden, Stimulation of DNA synthesis in murine lymphocytes by the drug swainsonine: immunomodulatory properties. *Biochem Biophys Res Commun* **150**, 615-625 (1988).
71. M. J. Humphries, K. Matsumoto, S. L. White, R. J. Molyneux, K. Olden, Augmentation of murine natural killer cell activity by swainsonine, a new antimetastatic immunomodulator. *Cancer Res* **48**, 1410-1415 (1988).
72. N. You *et al.*, Swainsonine inhibits growth and potentiates the cytotoxic effect of paclitaxel in hepatocellular carcinoma in vitro and in vivo. *Oncol Rep* **28**, 2091-2100 (2012).
73. M. J. Humphries, K. Matsumoto, S. L. White, K. Olden, Oligosaccharide modification by swainsonine treatment inhibits pulmonary colonization by B16-F10 murine melanoma cells. *Proc Natl Acad Sci U S A* **83**, 1752-1756 (1986).
74. J. W. Dennis, Effects of swainsonine and polyinosinic:polycytidylic acid on murine tumor cell growth and metastasis. *Cancer Res* **46**, 5131-5136 (1986).
75. I. Cornil, R. S. Kerbel, J. W. Dennis, Tumor cell surface beta 1-4-linked galactose binds to lectin(s) on microvascular endothelial cells and contributes to organ colonization. *J Cell Biol* **111**, 773-781 (1990).
76. P. E. Goss, J. Baptiste, B. Fernandes, M. Baker, J. W. Dennis, A phase I study of swainsonine in patients with advanced malignancies. *Cancer Res* **54**, 1450-1457 (1994).
77. P. E. Goss, C. L. Reid, D. Bailey, J. W. Dennis, Phase IB clinical trial of the oligosaccharide processing inhibitor swainsonine in patients with advanced malignancies. *Clin Cancer Res* **3**, 1077-1086 (1997).
78. P. E. Shaheen *et al.*, Phase II study of the efficacy and safety of oral GD0039 in patients with locally advanced or metastatic renal cell carcinoma. *Invest New Drugs* **23**, 577-581 (2005).
79. A. R. Almutairi, A. McBride, M. Slack, B. L. Erstad, I. Abraham, Potential Immune-Related Adverse Events Associated With Monotherapy and Combination Therapy of Ipilimumab, Nivolumab, and Pembrolizumab for Advanced Melanoma: A Systematic Review and Meta-Analysis. *Front Oncol* **10**, 91 (2020).
80. R. F. Wang, A special issue on cancer immunotherapy. *Cell Res* **27**, 1-2 (2017).
81. T. O. Akama *et al.*, Essential and mutually compensatory roles of {alpha}-mannosidase II and {alpha}-mannosidase IIx in N-glycan processing in vivo in mice. *Proc Natl Acad Sci U S A* **103**, 8983-8988 (2006).
82. R. S. Green *et al.*, Mammalian N-glycan branching protects against innate immune self-recognition and inflammation in autoimmune disease pathogenesis. *Immunity* **27**, 308-320 (2007).

83. J. B. Lowe, Glycosylation, immunity, and autoimmunity. *Cell* **104**, 809-812 (2001).
84. L. Zhang *et al.*, Lineage tracking reveals dynamic relationships of T cells in colorectal cancer. *Nature* **564**, 268-272 (2018).
85. X. Guo *et al.*, Global characterization of T cells in non-small-cell lung cancer by single-cell sequencing. *Nat Med* **24**, 978-985 (2018).
86. L. Cai *et al.*, LCE: an open web portal to explore gene expression and clinical associations in lung cancer. *Oncogene* **38**, 2551-2564 (2019).

Figure legend

Figure 1: *MAN2A1* is associated with T cell dysfunction. **A,** T cell dysfunction scores of N-glycan biosynthesis genes in the five TIDE core datasets. N-glycan biosynthesis genes were collected from KEGG_N_GLYCAN_BIOSYNTHESIS (hsa00510). Five data sets, representing five cancer types, had more than 1% of genes with FDR > 0.1. The gene list was ranked by the average T cell dysfunction score of the five cancer types. **B,** The association between the CTL level and overall survival for patients with different *MAN2A1* levels in TCGA melanoma cohort. The CTL infiltration level was estimated as the average expression level of *CD8A, CD8B, GZMA, GZMB and PRF1*. The association between the CTL level and overall survival was computed through the two-sided Wald test in the Cox-PH regression. "CTL Top" means samples have above-average CTL values among all samples, while 'CTL Bottom' means below average. Samples were split by the best separation strategy according to the *MAN2A1* expression coefficients in the Cox-PH regression model. **C,** Log2 fold change of genes with high dysfunction score in the public T cell co-culture screen data. MAGeCK was used to compute the log2 fold change for all gRNAs by comparing the experimental and control conditions.

Figure 2: *Man2a1*- null cancer cells are more sensitive to T cell-mediated killing. **A,** Western blot of MAN2A1 following genetic knockout. There are four independent CRISPR guides targeting *Man2a1* and control non-targeting *sgRosa26*. We selected the two guides with best knockout efficiency (the middle two lanes of sgMan2a1 group) for further functional study. **B,** Experimental schematic of T cell co-culture assay. *Man2a1*-null (GFP+) B16F10 cells and parental (GFP-) B16F10 were mixed and co-cultured with activated Pmel-1 T cells under IFN-γ induction for 24 hours. After co-culture, the ratio of GFP+ cells to parental cells (GFP-) was determined by flow cytometry. **C,** The effect of *Man2a1* knockout on T cell-mediated tumor killing. The y-axis is the ratio of GFP+ cells to GFP- cells normalized to the untreated condition. Two-way ANOVA with Benjamini-Hochberg post-test comparison was used to determine statistical significance (*** $p<0.001$). Values represents mean ± s.d.

Figure 3: *Man2a1* knockout changes glycol-metabolism and glycosylation of PD-L1. A, Volcano plot for differentially expressed genes in *Man2a1*-null B16F10 cells compared to control cells. Log2 fold change and adjusted p-values were computed by DESeq2. Annotated genes represent down regulated genes (fold change < -1.2 & adj.p.value < 0.1) which are enriched in Glycolysis, Starch and sucrose metabolism pathways or the others (top 5 hits with the most significant adjust p value). **B,** Gene ontology analysis for down regulated genes between *Man2a1*-null and control B16F10 cells. "MAGeCKFlute" R package was used to perform the enrichment analysis. **C** and **D,** Bar plot of the relative abundance of representative N-glycans among total N-glycans. (**C**), Hybrid type; (**D**), Complex type. **E,** Western blot analysis of PD-L1 expression in *MAN2A1*-knockout and control A375 cells treated with/without swainsonine. **F,** Western blot analysis of PD-L1 expression in MAN2A1-knockout and control Colo205 cells treated with/without swainsonine and PNGase F.

Figure 4: *Man2a1* loss in cancer cells enhances anti-PD-L1 response. A, mRNA levels of *Man2a1*-knockout gene signature (down regulated genes in *Man2a1* knockout cells) between the responding versus non-responding pretreatment tumors. ssGSEA was used to calculate the single sample signature score. Two-sided Student's t-test was used to compute the p-value. **B,** Overall survival of anti-PD-L1-treated urothelial cancer patients harboring high (above the group median) or low (below the group median) expression level of *Man2a1*-knockout gene signature. Log-rank test was used to compute the p-value in survival analysis. **C,** Tumor volume of control and *Man2a1*-null B16F10 tumors in C57BL/6 mice treated with IgG isotype control or anti-PD-L1. N = 9 mice for each group. ****p < 0.0001; ***p < 0.001; **p < 0.01, *p < 0.05 by two-way ANOVA. Data are mean ± s.e.m. **D,** Survival analysis of control and *Man2a1*-null B16F10 tumors treated with IgG isotype control or anti-PD-L1. N= 9 mice for each group. *p < 0.05 by log-rank test.

Figure 5: *Man2a1* knockout increases the cytotoxic immune cell infiltration and activities. A, Gene sets enriched in *Man2a1* knockout tumors treated with PD-L1 blockade compared to control tumors with anti-PD-L1 treatment. Pre-ranked Gene set enrichment analysis (GSEA) analysis was used to calculate the enrichment. **B,** Heat map showing expression value (z-score based on TPM) of antigen presentation, inflammatory response, and T cell activation genes in *Man2a1*-null or control B16F10 tumors treated with IgG isotype control or anti-PD-L1. **C-E,** Flow cytometry of immune populations from control and *Man2a1*-null B16F10 tumors treated with IgG or anti-PD-L1. (**C**), CD45; (**D**), CD3; (**E**), CD8. Data are mean ± s.d, representative of at least two independent experiments. N = 6 mice for each group. ****p < 0.0001; ***p < 0.001; **p < 0.01, *p < 0.05 by one-way ANOVA with Tukey's multiple comparisons test. **F** and **G,** IFN-γ and TNF-α protein levels in tumor lysates of *Man2a1* null and control B16F10 tumors. (**F**), IFN-γ protein; (**G**), TNF- α protein. N = 3 mice for each group. Data are mean ± s.d, representative of at least two independent experiments. ****p < 0.0001; ***p < 0.001; **p < 0.01, *p < 0.05 by one-way ANOVA with Tukey's multiple comparisons test.

Figure 6: Pharmacological inhibition of *Man2a1* sensitizes tumors to anti-PD-L1. A, B16F10 tumor volume in response to swainsonine and anti-PD-L1. N = 10 mice per group. Data are shown as the mean ± s.e.m. *p < 0.05; **p < 0.01; ***p < 0.001; ****p < 0.0001 by two-way ANOVA. **B,** Survival curve of B16F10 tumors in response to swainsonine and anti-PD-L1. N = 10 mice per group. log-rank test, *p < 0.05. **C,** LLC tumor volume in response to swainsonine and anti–PD-L1. N = 10 mice per group. Data are shown as the mean ± s.e.m. *p < 0.05; **p < 0.01; ***p < 0.001; ****p < 0.0001 by two-way ANOVA. **D,** Survival curve of LLC tumors in response to swainsonine and anti–PD-L1. N = 10 mice per group. log-rank test, *p < 0.05. **E** and **F,** Flow cytometry of immune populations from B16F10 tumors treated with different drug combinations. (**E**), CD3; (**F**), CD8. Data are mean ± s.d. ****p < 0.0001; ***p < 0.001; **p < 0.01, *p < 0.05 by one-way ANOVA with Tukey's multiple comparisons test. **G,** Gene sets enriched in B16F10 tumors treated with combined anti-PD-L1 and swainsonine compared to tumors treated with anti-PD-L1. Pre-ranked Gene set enrichment analysis (GSEA) analysis was used to calculate the enrichment. **H,** Heat map showing expression value (z-score based on TPM) of T cell activation and leukocyte mediated cytolysis genes in

B16F10 tumors treated with different drug combinations. **I** and **J,** IFN-γ and TNF- α protein levels in tumor lysates of B16F10 tumors treated with different drug combinations. (**I**), IFN-γ protein; (**J**), TNF- α protein. N = 4 mice for each group. Data are mean ± s.d, representative of at least two independent experiments. ****p < 0.0001; ***p < 0.001; **p < 0.01, *p < 0.05 by one-way ANOVA with Tukey's multiple comparisons test.

Figure 1

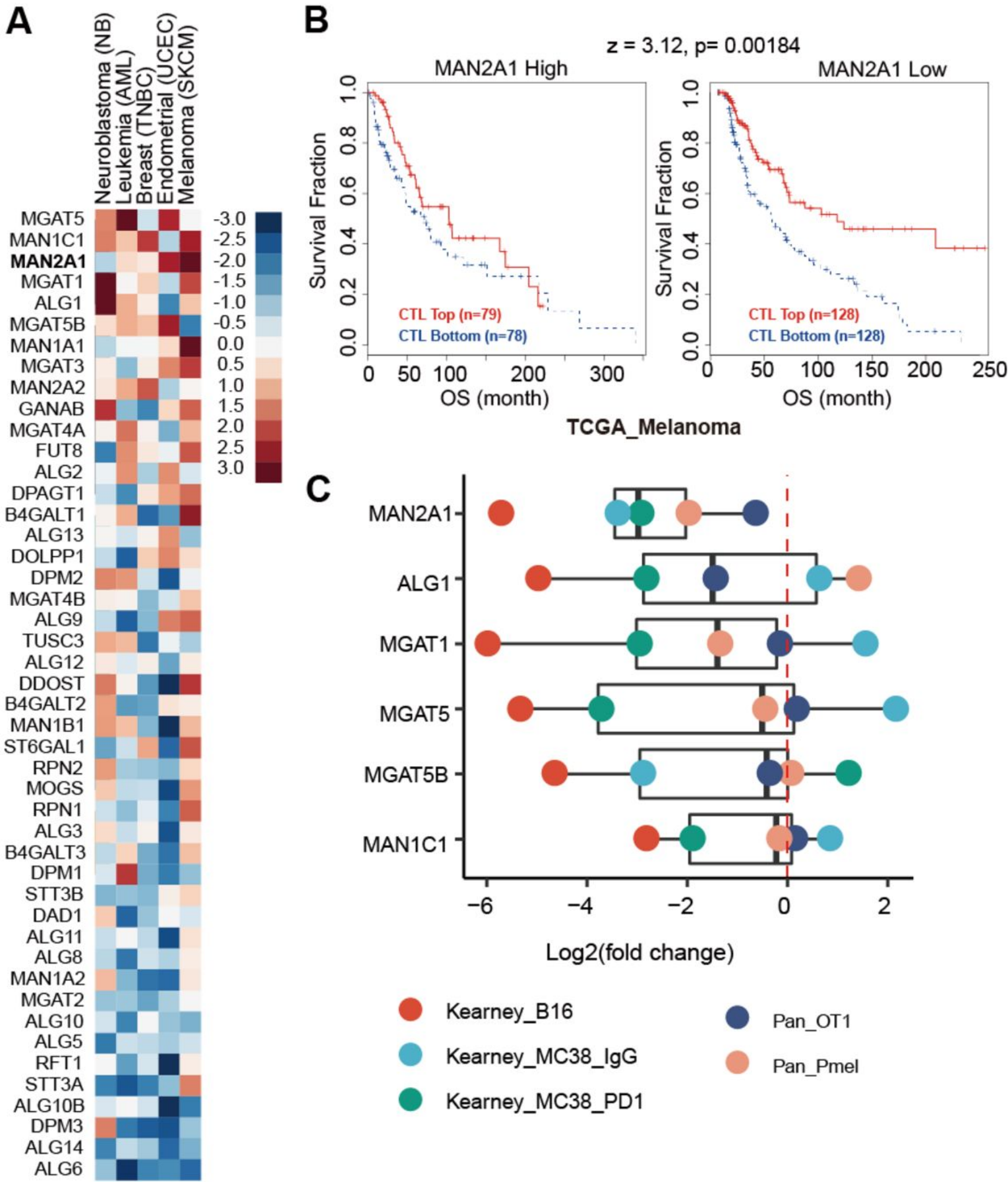
A
Neuroblastoma (NB)
Leukemia (AML)
Breast (TNBC)
Endometrial (UCEC)
Melanoma (SKCM)
MGAT5
MAN1C1
MAN2A1
MGAT1
ALG1
MGAT5B
MAN1A1
MGAT3
MAN2A2
GANAB
MGAT4A
FUT8
ALG2
DPAGT1
B4GALT1
ALG13
DOLPP1
DPM2
MGAT4B
ALG9
TUSC3
ALG12
DDOST
B4GALT2
MAN1B1
ST6GAL1
RPN2
MOGS
RPN1
ALG3
B4GALT3
DPM1
STT3B
DAD1
ALG11
ALG8
MAN1A2
MGAT2
ALG10
ALG5
RFT1
STT3A
ALG10B
DPM3
ALG14
ALG6
-3.0
-2.5
-2.0
-1.5
-1.0
-0.5
0.0
0.5
1.0
1.5
2.0
2.5
3.0
B
z = 3.12, p= 0.00184
MAN2A1 High
MAN2A1 Low
Survival Fraction
CTL Top (n=79)
CTL Bottom (n=78)
CTL Top (n=128)
CTL Bottom (n=128)
OS (month)
TCGA_Melanoma
C
MAN2A1
ALG1
MGAT1
MGAT5
MGAT5B
MAN1C1
Log2(fold change)
Kearney_B16
Kearney_MC38_IgG
Kearney_MC38_PD1
Pan_OT1
Pan_Pmel

Figure 2

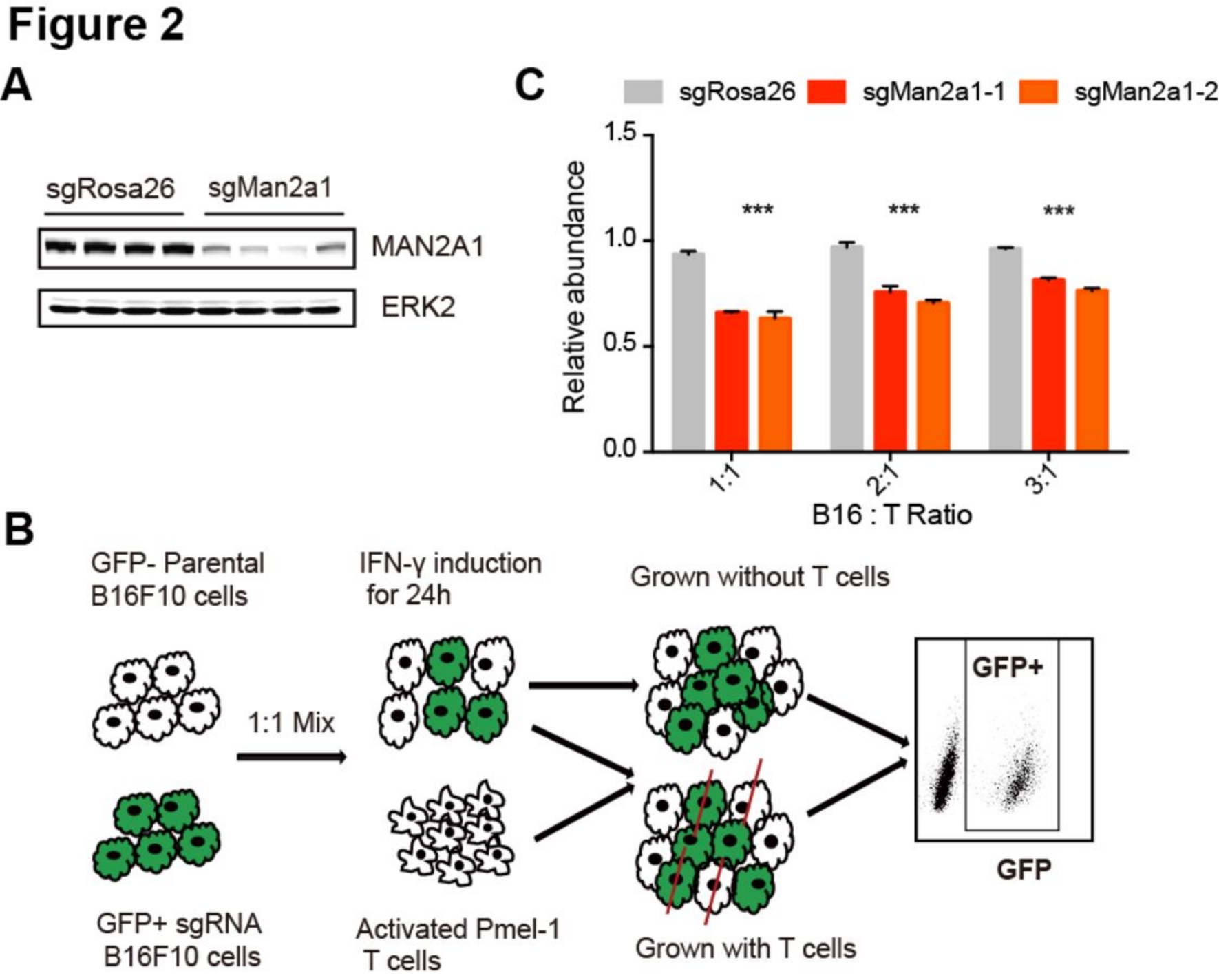
A
sgRosa26
sgMan2a1
MAN2A1
ERK2
C
sgRosa26
sgMan2a1-1
sgMan2a1-2
Relative abundance
1.5
1.0
0.5
0.0
***
***
***
1:1
2:1
3:1
B16 : T Ratio
B
GFP- Parental
B16F10 cells
1:1 Mix
GFP+ sgRNA
B16F10 cells
IFN-γ induction
for 24h
Activated Pmel-1
T cells
Grown without T cells
Grown with T cells
GFP+
GFP

Figure 3

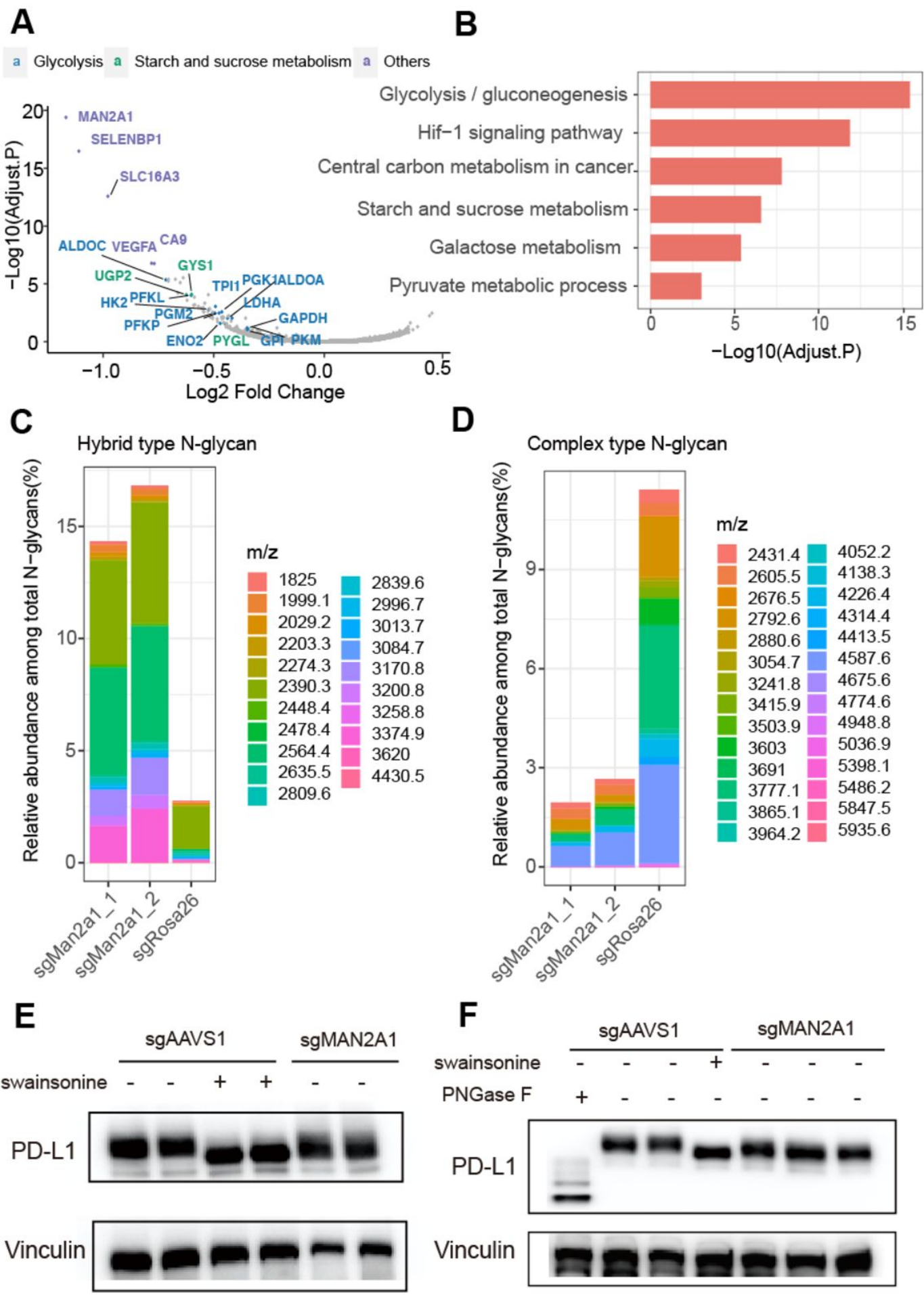
A
Glycolysis
Starch and sucrose metabolism
Others
MAN2A1
SELENBP1
SLC16A3
ALDOC
VEGFA
CA9
GYS1
UGP2
TPI1
PGK1
ALDOA
HK2
PFKL
LDHA
PGM2
PFKP
GAPDH
ENO2
PYGL
GPI
PKM
−Log10(Adjust.P)
Log2 Fold Change
B
Glycolysis / gluconeogenesis
Hif−1 signaling pathway
Central carbon metabolism in cancer
Starch and sucrose metabolism
Galactose metabolism
Pyruvate metabolic process
−Log10(Adjust.P)
C
Hybrid type N-glycan
Relative abundance among total N−glycans(%)
m/z
1825
1999.1
2029.2
2203.3
2274.3
2390.3
2448.4
2478.4
2564.4
2635.5
2809.6
2839.6
2996.7
3013.7
3084.7
3170.8
3200.8
3258.8
3374.9
3620
4430.5
sgMan2a1_1
sgMan2a1_2
sgRosa26
D
Complex type N-glycan
Relative abundance among total N−glycans(%)
m/z
2431.4
2605.5
2676.5
2792.6
2880.6
3054.7
3241.8
3415.9
3503.9
3603
3691
3777.1
3865.1
3964.2
4052.2
4138.3
4226.4
4314.4
4413.5
4587.6
4675.6
4774.6
4948.8
5036.9
5398.1
5486.2
5847.5
5935.6
sgMan2a1_1
sgMan2a1_2
sgRosa26
E
sgAAVS1
sgMAN2A1
swainsonine
PD-L1
Vinculin
F
sgAAVS1
sgMAN2A1
swainsonine
PNGase F
PD-L1
Vinculin

Figure 4

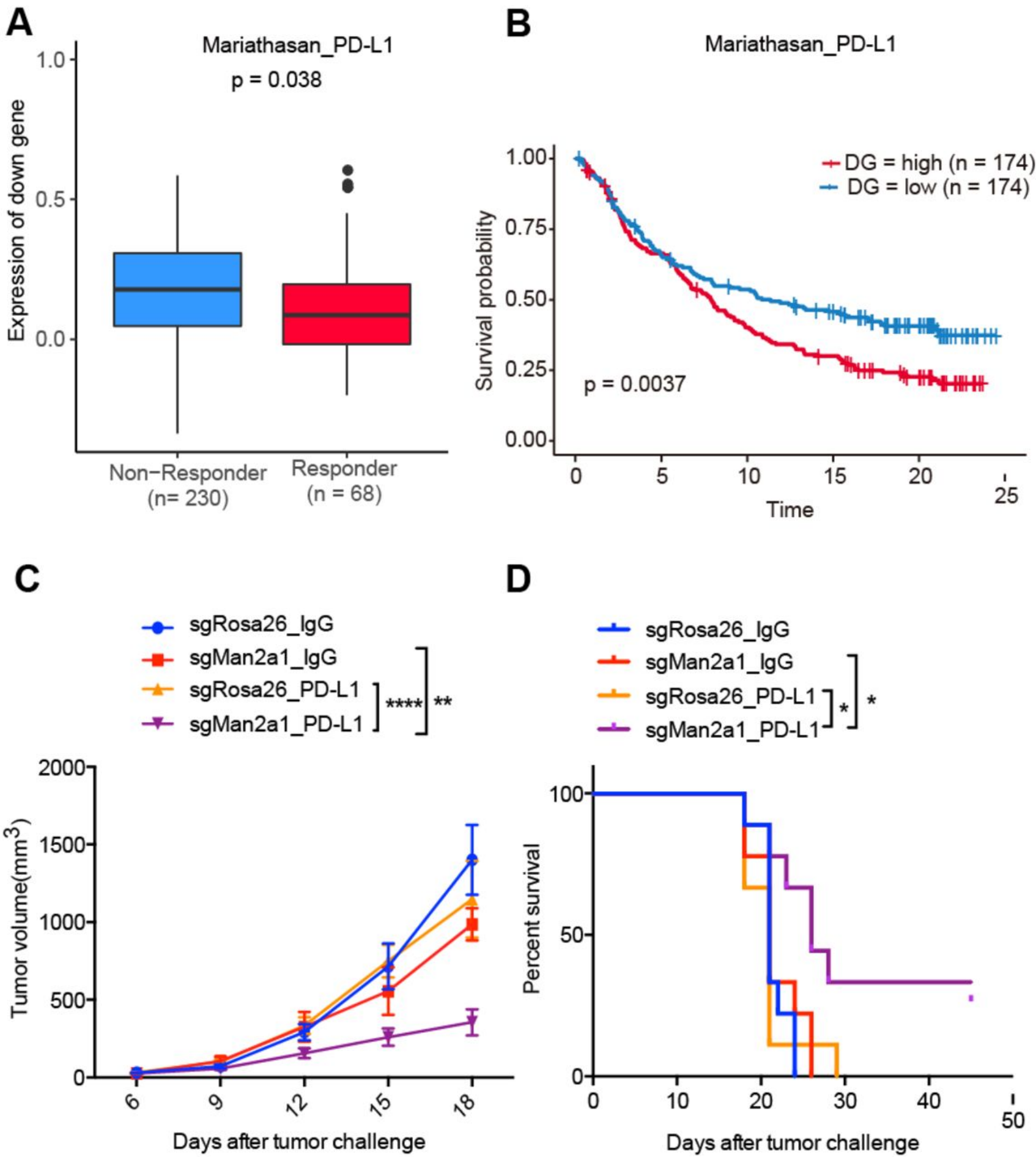
A
Mariathasan_PD-L1
p = 0.038
Expression of down gene
1.0
0.5
0.0
Non−Responder
(n= 230)
Responder
(n = 68)
B
Mariathasan_PD-L1
DG = high (n = 174)
DG = low (n = 174)
Survival probability
1.00
0.75
0.50
0.25
0.00
p = 0.0037
0
5
10
15
20
25
Time
C
sgRosa26_IgG
sgMan2a1_IgG
sgRosa26_PD-L1
sgMan2a1_PD-L1
****
**
Tumor volume(mm3)
2000
1500
1000
500
0
6
9
12
15
18
Days after tumor challenge
D
sgRosa26_IgG
sgMan2a1_IgG
sgRosa26_PD-L1
sgMan2a1_PD-L1
*
*
Percent survival
100
50
0
0
10
20
30
40
50
Days after tumor challenge

Figure 5

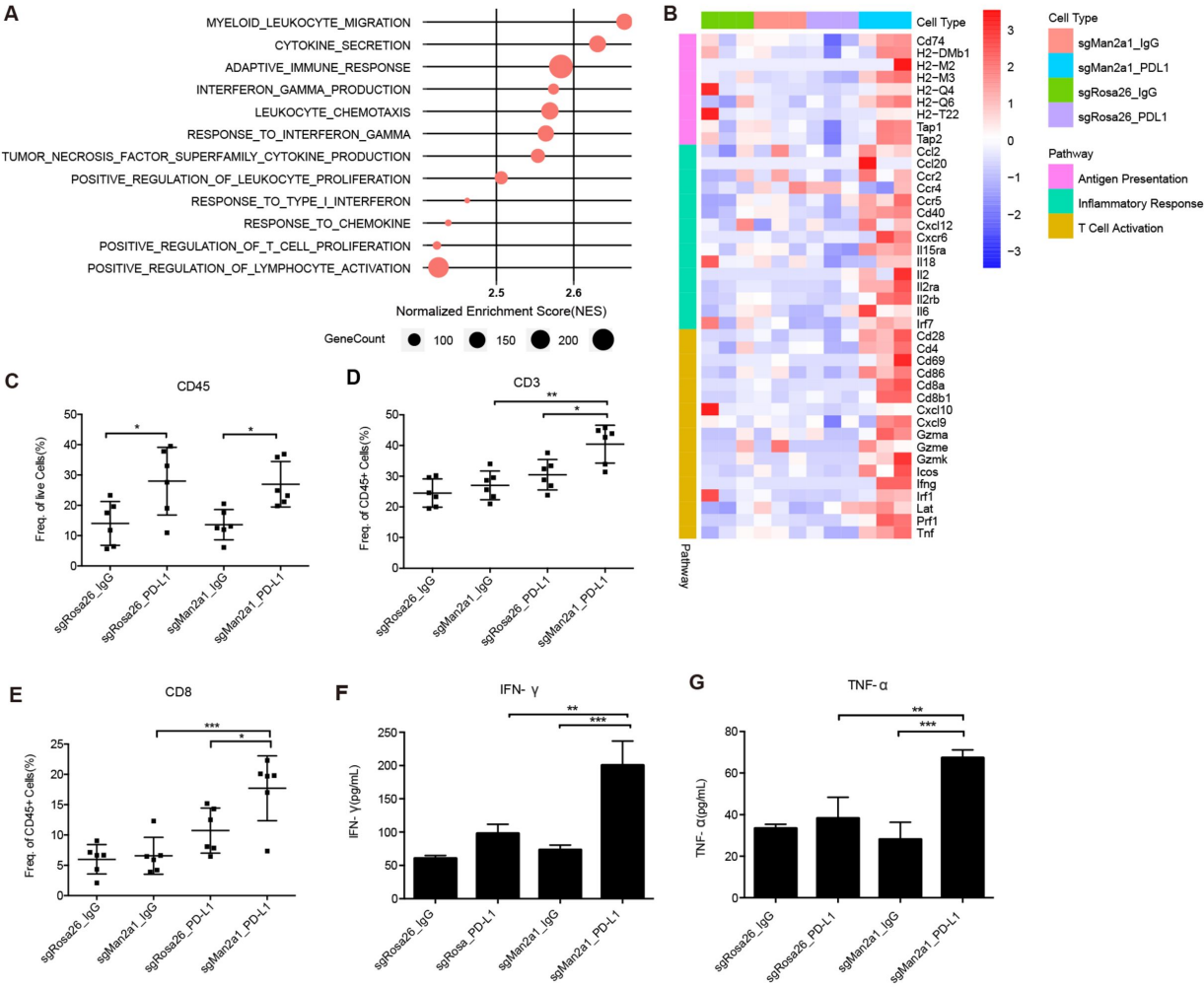
A
MYELOID_LEUKOCYTE_MIGRATION
CYTOKINE_SECRETION
ADAPTIVE_IMMUNE_RESPONSE
INTERFERON_GAMMA_PRODUCTION
LEUKOCYTE_CHEMOTAXIS
RESPONSE_TO_INTERFERON_GAMMA
TUMOR_NECROSIS_FACTOR_SUPERFAMILY_CYTOKINE_PRODUCTION
POSITIVE_REGULATION_OF_LEUKOCYTE_PROLIFERATION
RESPONSE_TO_TYPE_I_INTERFERON
RESPONSE_TO_CHEMOKINE
POSITIVE_REGULATION_OF_T_CELL_PROLIFERATION
POSITIVE_REGULATION_OF_LYMPHOCYTE_ACTIVATION
2.5
2.6
Normalized Enrichment Score(NES)
GeneCount
100
150
200
B
Cell Type
Cd74
H2−DMb1
H2−M2
H2−M3
H2−Q4
H2−Q6
H2−T22
Tap1
Tap2
Ccl2
Ccl20
Ccr2
Ccr4
Ccr5
Cd40
Cxcl12
Cxcr6
Il15ra
Il18
Il2
Il2ra
Il2rb
Il6
Irf7
Cd28
Cd4
Cd69
Cd86
Cd8a
Cd8b1
Cxcl10
Cxcl9
Gzma
Gzme
Gzmk
Icos
Ifng
Irf1
Lat
Prf1
Tnf
Pathway
3
2
1
0
−1
−2
−3
Cell Type
sgMan2a1_IgG
sgMan2a1_PDL1
sgRosa26_IgG
sgRosa26_PDL1
Pathway
Antigen Presentation
Inflammatory Response
T Cell Activation
C
CD45
Freq. of live Cells(%)
sgRosa26_IgG
sgRosa26_PD-L1
sgMan2a1_IgG
sgMan2a1_PD-L1
D
CD3
Freq. of CD45+ Cells(%)
sgRosa26_IgG
sgMan2a1_IgG
sgRosa26_PD-L1
sgMan2a1_PD-L1
E
CD8
Freq. of CD45+ Cells(%)
sgRosa26_IgG
sgMan2a1_IgG
sgRosa26_PD-L1
sgMan2a1_PD-L1
F
IFN- γ
IFN- γ(pg/mL)
sgRosa26_IgG
sgRosa_PD-L1
sgMan2a1_IgG
sgMan2a1_PD-L1
G
TNF- α
TNF- α(pg/mL)
sgRosa26_IgG
sgRosa26_PD-L1
sgMan2a1_IgG
sgMan2a1_PD-L1

Figure 6

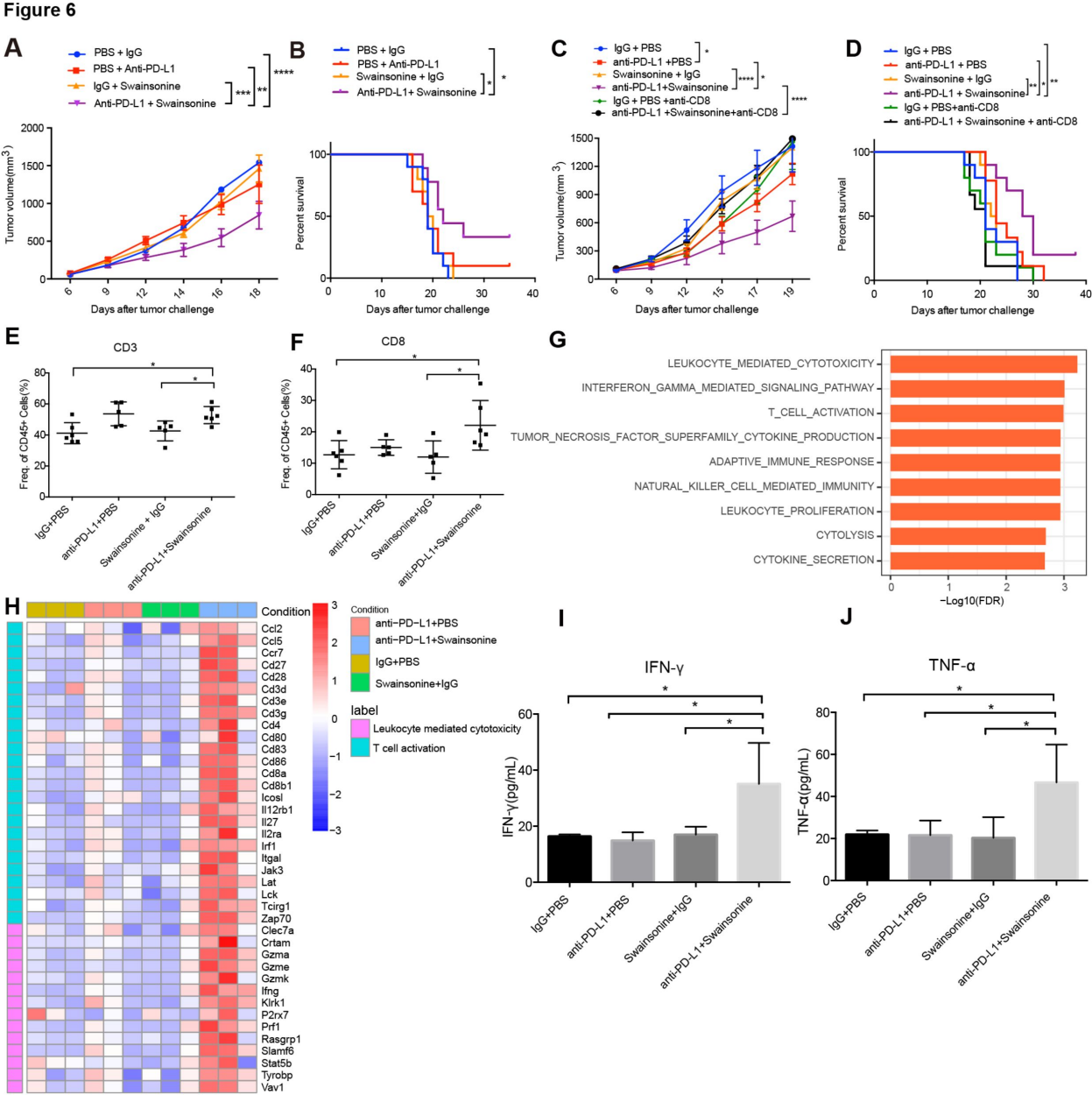
A
PBS + IgG
PBS + Anti-PD-L1
IgG + Swainsonine
Anti-PD-L1 + Swainsonine
Tumor volume(mm3)
Days after tumor challenge
B
PBS + IgG
PBS + Anti-PD-L1
Swainsonine + IgG
Anti-PD-L1+ Swainsonine
Percent survival
Days after tumor challenge
C
IgG + PBS
anti-PD-L1 +PBS
Swainsonine + IgG
anti-PD-L1+Swainsonine
IgG + PBS +anti-CD8
anti-PD-L1 +Swainsonine+anti-CD8
Tumor volume(mm 3)
Days after tumor challenge
D
IgG + PBS
anti-PD-L1 + PBS
Swainsonine + IgG
anti-PD-L1 + Swainsonine
IgG + PBS+anti-CD8
anti-PD-L1 + Swainsonine + anti-CD8
Percent survival
Days after tumor challenge
E
CD3
Freq. of CD45+ Cells(%)
IgG+PBS
anti-PD-L1+PBS
Swainsonine + IgG
anti-PD-L1+Swainsonine
F
CD8
Freq. of CD45+ Cells(%)
IgG+PBS
anti-PD-L1+PBS
Swainsonine+IgG
anti-PD-L1+Swainsonine
G
LEUKOCYTE_MEDIATED_CYTOTOXICITY
INTERFERON_GAMMA_MEDIATED_SIGNALING_PATHWAY
T_CELL_ACTIVATION
TUMOR_NECROSIS_FACTOR_SUPERFAMILY_CYTOKINE_PRODUCTION
ADAPTIVE_IMMUNE_RESPONSE
NATURAL_KILLER_CELL_MEDIATED_IMMUNITY
LEUKOCYTE_PROLIFERATION
CYTOLYSIS
CYTOKINE_SECRETION
−Log10(FDR)
H
Condition
anti−PD−L1+PBS
anti−PD−L1+Swainsonine
IgG+PBS
Swainsonine+IgG
label
Leukocyte mediated cytotoxicity
T cell activation
Ccl2
Ccl5
Ccr7
Cd27
Cd28
Cd3d
Cd3e
Cd3g
Cd4
Cd80
Cd83
Cd86
Cd8a
Cd8b1
Icosl
Il12rb1
Il27
Il2ra
Irf1
Itgal
Jak3
Lat
Lck
Tcirg1
Zap70
Clec7a
Crtam
Gzma
Gzme
Gzmk
Ifng
Klrk1
P2rx7
Prf1
Rasgrp1
Slamf6
Stat5b
Tyrobp
Vav1
I
IFN-γ
IFN-γ(pg/mL)
IgG+PBS
anti-PD-L1+PBS
Swainsonine+IgG
anti-PD-L1+Swainsonine
J
TNF-α
TNF-α(pg/mL)
IgG+PBS
anti-PD-L1+PBS
Swainsonine+IgG
anti-PD-L1+Swainsonine